Filamentation nonlinear optics: a new frontier

S.L. Chin[*a], F. Théberge[*a,b], H. Xu[a], W. Liu[a,c], J.-F. Daigle[a], Q. Luo[a], S.M. Sharifi[a], Y. Chen[a], N. Aközbek[d], A. Becker[e], C. Marceau[a], P. Tremblay-Simard[a], Y. Kamali[a], A. Azarm[a], J. Bernhardt[a], P. Mathieu[b], G. Roy[b], J.-R Simard[b]

[a] Centre d'Optique, Photonique et Laser (COPL) and Département de physique, de génie physique et d'optique, Université Laval, Québec, Québec G1K 7P4, Canada;

[b] Defense Research and Development Canada-Valcartier, 2459 Pie-XI Blvd North, Québec, Québec, G3J 1X5, Canada;

[c] Institute of Modern Optics, Nankai University, Tianjin, 300071, China;

[d] Time Domain Corporation, Cummings Research Park, 7057 Old Madison Pike, Suite 250, Huntsville, AL 35806, USA;

[e] Max-Planck-Institut für Physik komplexer Systeme, Nöthnitzer Str. 38, 01187 Dresden, Germany

ABSTRACT

The filament core of a femtosecond laser pulse propagating in an optical medium has extra-ordinary quality for exploitation that includes high quality tunable pulse generation from the UV to the THz. The peak intensity inside the filament is also high enough to dissociate/ionize any molecules resulting in remarkably distinct spectra which can be use for remote sensing of Chem-bio agent.

Keywords: Nonlinear optics, self-focusing, plasma, LIDAR, teledetection

1. INTRODUCTION

The physics of femtosecond laser filamentation is by now basically understood [1]. A new application in the self-compression of the filamenting pulse into a few-cycle-pulse has emerged [2-4] and has attracted a lot of interest for the generation of energetic pulses down to the single cycle regime [5, 6]. This is just one of the consequences of the self-transformation of the laser pulse during filamentation. Another consequence is the self-transformation into a white light laser pulse [7-9] whose spectral content spans from 230 nm to 4.5 μm [10, 11]. In the first part of this work, we like to show yet another consequence of filamentation; i.e. the filament core is very stable and is of high spatial quality. Proper sampling of this core zone through *nonlinear* processes could result in very high quality outcome. The idea to sample the filament core through nonlinear interaction is to avoid the participation of the reservoir [9, 12, 13]. Since the filament core has a constant high intensity due to intensity clamping [14-16] and the intensity distribution inside the core is naturally homogeneous due to a self-filtering process (see below), any nonlinear optical interaction that samples only the core will end up with an efficient output (because of high intensity) whose fluctuation will be dramatically reduced (due to intensity clamping) and whose spatial quality becomes extremely good (due to self-filtering). This is contrary to the normal wisdom that any nonlinear interaction will result in a large fluctuation of the signal/outcome as compared to linear interaction. We call this 'filamentation nonlinear optics'.

Such filamentation can also be controlled, in principle, to occur at a distance as far as a few kilometers in the atmosphere [1, 17]. Inside the filament, the peak intensity is clamped around 5×10^{13} W/cm^2 [1] and is high enough to dissociate/ionize gas molecules, to explode fine particles (dusts and aerosols) and to induce 'partial' breakdown on solid targets. The interaction of the strong field inside the filament in air with molecules would result in "clean" fluorescence emissions practically free of plasma continuum. We further discovered that such 'clean' fluorescence is a general phenomenon in the interaction of the strong field inside the filament and all targets ranging from gases, vapors, aerosols to solids. Furthermore, such 'clean' fluorescence is unique from agent to agent; i.e. each agent will result in its own fingerprint fluorescence.

[*] Email : slchin@phy.ulaval.ca, francis.theberge.aerex@drdc-rddc.gc.ca

International Conf. on Lasers, Applications, and Technologies 2007: Environmental Monitoring and Ecological Applications; Optical Sensors in Bio, Chemical, and Engineering Technologies; and Femtosecond Laser Pulse Filamentation, edited by G. G. Matvienko, et al., Proc. of SPIE Vol. 6733, 67332B, (2007) · 0277-786X/07/$18 · doi: 10.1117/12.753141

This paper gives a physical discussion of the above processes using air as the propagating medium. It is supported by some experimental data on four-wave mixing inside the filament in air. It is applicable to other nonlinear processes in other optical media such as writing waveguide in glasses since the physics of filamentation is essentially universal [1]. Its limitation is also discussed using third-harmonic generation in air as an example. We have also carried out experiments for the remote generation of filament in the atmosphere and systematic experimental studies inside the laboratory environment by measuring the characteristic fingerprint fluorescence of representative target examples. Extrapolation of the laboratory results to remote targets using the LIDAR equation shows that it is feasible to remotely detect all these agents in the range of kilometers. This opens up the door towards remote detection of targets related to safety, security and pollution.

2. PHYSICS OF FILAMENTATION

Filamentation is the result of the slice-by-slice self-focusing process [18]. It starts with the strongest slice at the peak of the pulse. When this slice self-focuses in air, its intensity increases continuously until it is high enough to generate a weak plasma through tunnel ionization [19] of the air molecules. Because the index of refraction of the plasma is smaller than unity, the focusing slice will diverge (be de-focused) out of the self-generated plasma. This balancing act between self-focusing and self-defocusing results in a limited peak intensity at the self-focal zone. Successive slices at the front part of the pulse will self-focus in the same way and will always end up with the same limited peak intensity because the ionization processes at the high intensity zones of all slices are identical. We call this intensity clamping. The clamped intensity is of the order of 5×10^{13} W/cm^2 in air [14, 15]. The series of self-foci constitute what we call by a filament. The slices at the back part of the pulse will always self-focus into the plasma left behind by the front part of the pulse before the intensity reaches the clamped intensity. They will interact with the plasma and be de-focused outward resulting eventually in self-steepening of the back part of the pulse [20]. The energy of all these diverging slices from the front and back parts of the pulse constitutes the so-called reservoir [9, 12, 13]. The intensity and energy distribution of the reservoir will not be homogeneous because there is a continuous exchange of energy between the reservoir and the self-focal zone.

3. SELF-SPATIAL FILTERING

The above description pertains to the filamentation of an initially ideal pulse whose transverse intensity and fluence distribution is Gaussian. However, in all real experimental cases, such an ideal pulse could never be obtained. The imperfect transverse intensity and fluence distribution of a real pulse from any experiment is essentially the superposition of the fundamental and other higher order spatial modes. Self-focusing effect will concentrate the fundamental mode on the propagation axis and the higher-order modes occupy a larger cross-section similar to the geometrical focusing of a laser beam composed of many modes. Figure 1 shows the numerically simulated normalized intensity distribution across the diameter of an assumed CW beam propagating in air at two distances. The propagation is described by the classic nonlinear wave equation:

$$2ik_0 \frac{\partial A}{\partial z} + \Delta_\perp A + 2k_0^2 \Delta n A = 0 \qquad (1)$$

where A represents the amplitude of the light field, k_0 denotes the wave number of the beam and Δn corresponds to the optical Kerr effect induced nonlinear refractive index. The initial laser beam is Gaussian and has a diameter of 1 mm at $1/e^2$ level. Its power is three times the critical power for self-focusing. To demonstrate the self-filtering process during self-focusing, ten randomly distributed perturbations are introduced into this smooth beam profile. Each perturbation is 200 μm in diameter, while its peak intensity is ten percent of the initial local intensity. Such an inhomogeneous intensity distribution $I(x, y = 0)$ ($x = 0$ and $y = 0$ is the coordinate of the center of the beam) at z = 0 cm is shown as thin line in Fig. 2. The calculation is stopped at z = 32 cm, where the intensity has reached 5×10^{13} W/cm^2, being the clamped intensity in air [14, 15]. The distribution $I(x, y = 0)$ (thick line) after 32 cm propagation, is very smooth at the center (core) while all the higher order modes diverge out and are several orders of magnitude lower than the central peak. Figure 1 is a theoretical justification of the above idea that the filament core has a high quality intensity (and hence fluence) distribution.

At the self-focal zone, the high intensity of the fundamental mode will tunnel ionize [19] the air molecules resulting in a weak plasma which defocuses the laser slice. Since tunnel ionization is a uni-molecular process and the plasma density is low (about 10^{16} cm^{-3} [21-23], three orders of magnitude lower than the density of air), very little energy of the laser is consumed [18] and the resulting weak electron distribution will be homogeneous and would not disrupt the homogeneous intensity and fluence distribution of the fundamental mode at the self-focal zone; i.e. the high quality filament core is preserved. Hence, if the laser peak power of such a pulse was not too high so that multiple filaments were not yet induced, at the self-focal region, the intensity and fluence distribution would correspond to those of the fundamental mode. The plasma will defocus the higher order modes more than the fundamental is defocused. This is similar to spatial filtering of long laser pulses using a relatively thick-wall glass conic pinhole of an appropriate diameter at the focus of a lens with the large opening of the cone facing the lens. The fundamental mode will go through the pinhole while the higher order spatial modes will be refracted away by the thick wall of the cone. The central part of this beam (fundamental mode) can then be separated in the far-field from the higher order modes.

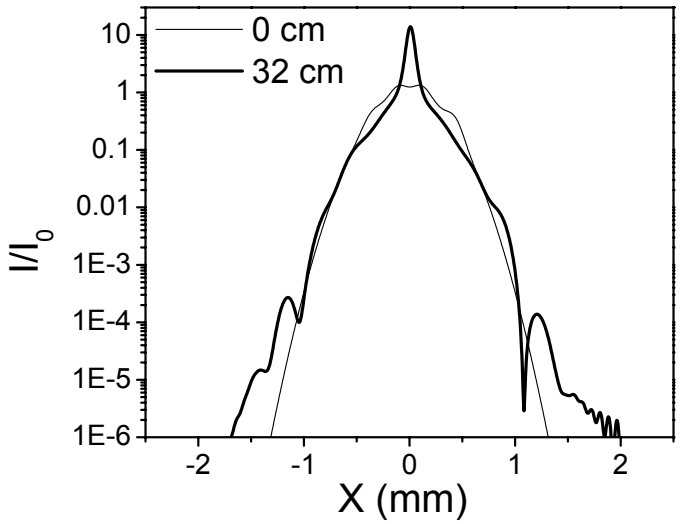

Fig. 1. Simulated intensity distribution of an initially distorted pulse profile at two propagation distances in air. Thin line: z = 0 cm; thick line: z = 32 cm.

4. PHYSICAL VISUALIZATION

Consequently, during filamentation, at any position along the propagation axis, in the front part of the pulse, there is one self-focal zone (core) having a constant peak, high, clamped intensity with a homogeneous spatial intensity and fluence distribution corresponding to that of the fundamental spatial mode. This 'high quality core' is surrounded by a 'low quality reservoir' whose intensity is not uniform across the entire reservoir zone. The core moves forward in the front part of the pulse while the pulse propagates. The core conserves the same peak clamped intensity with always a homogeneous intensity and fluence spatial distribution while the reservoir fluctuates in intensity in space and time during propagation.

Thus, any *linear* interaction with this pulse will unavoidably end up with an output that is *linearly* proportional to the whole filamenting pulse (core plus reservoir). The *linear* output conserves the quality of the mixture of the 'good quality' core and the 'bad quality' reservoir. However, if one could sample only the core zone, the output would be very good in quality. This could be achieved through nonlinear interaction with the pulse such as any parametric process.

4.1 Example 1

As a first example, we consider self-phase modulation in the high intensity core which is created always at the front part of the pulse. Because the front part of the pulse always encounters the neutral medium during propagation, self-phase

modulation would result in a symmetrical spectral broadening towards the red and blue sides of the pump wavelength. Since self-phase modulation is a third order process, it essentially samples the core zone. The intensity/fluence distribution of any color of such shifts should reflect the intensity distribution of the high quality core; i.e. each new color should show a good mode pattern. However, since the back part of the pulse always interacts with the plasma left behind by the front part, self-phase modulation inside the plasma and eventually self-steepening would give rise to strong blue shifts whose intensities would not be stable because there is no stabilizing process such as intensity clamping. Thus, the intensity/fluence distribution of the color at the blue side of the pump wavelength would not reflect a good mode pattern. Fig. 2 shows the transverse fluence distributions (patterns) of three colors after the filamentation of a 45 fs/5 mJ Ti-sapphire laser pulse in air taken at 30 m from the output of the laser system. Fig. 2a is the initial irregular beam pattern at 800 nm. Fig. 2b shows the very good beam pattern at the red side (950 nm) of the pump. This latter is due to pure self-phase modulation in the neutral that samples the filament core and hence reflects the good beam quality of the filament core. Fig. 2c shows an example at the blue side (600nm). The bad beam quality is obvious.

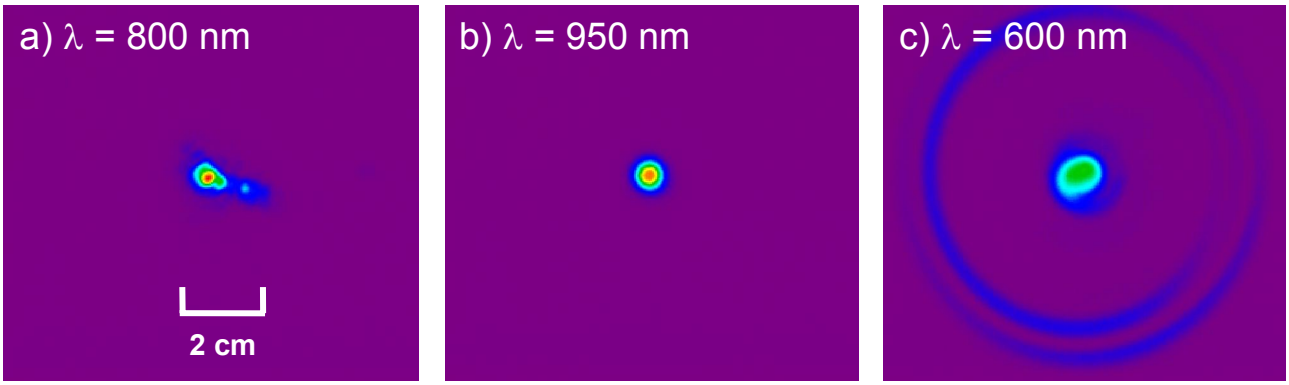

Fig. 2. CCD camera recorded patterns at various wavelengths a) 800nm, b) 950nm and c) 600nm after propagation in air of a 800nm, 45 fs laser pulse.

4.2 Example 2

A second example is the output of four-wave mixing (4WM) inside a filament in air [23]. The experiment was performed using a near-infrared (NIR) 800nm Ti-sapphire femtosecond laser pulse (45 fs, 2 mJ/pulse). It was focused into air by long focal length lenses (f = 0.8 m or 4 m) generating a filament. A second tunable infrared (IR) 1 to 2 μm femtosecond laser pulse emitted from an optical parametric amplifier pumped by part of the NIR 800nm beam was superposed concentrically with the NIR laser pulse and the temporal delay between the IR and the NIR laser pulses was controlled by an optical delay line. Due to the strong non-linear interaction between the IR and NIR laser pulses during their co-propagation, efficient third-order parametric effects occurred within the filament zone. The output frequency of the generated pulse is determined by $\omega_{4WM} = 2\omega_{NIR} - \omega_{IR}$ where 4WM refers to four-wave mixing. Beyond the filament, a dichroic mirror was used to suppress the pump pulses and transmitted the efficiently generated 4WM pulse.

The ultrashort 4WM pulses show a remarkable low energy fluctuation and possess an excellent mode quality [23]. Figure 3a shows the distorted NIR fluence distribution before the filament and Fig. 3b shows the exceptional beam quality profile of the 4WM pulse generated through filamentation. The 4WM fluence distribution was smooth, centered on the propagation axis and similar to a symmetric Gaussian profile. The parameters of the 4WM beam diffracting out of the filament are very similar to those of a near diffraction limited Gaussian beam whose M^2 value was measured to be less than 1.01 while the initial quality factor of the NIR beam was M^2 =1.3. The excellent laser profile of the generated 4WM pulse is due to the spatial self-filtering process occurring in the filament. For laser pulses having power higher than the critical power for self-focusing, the transverse profile of the beam evolves into a circularly symmetric high constant (clamped) intensity zone surrounded by a noisy background of light (energy reservoir). Since the 4WM pulse is mainly generated in the high intensity zone of the filament (i.e. sampling the filament core using nonlinear optics), the 4WM pulse acquires a profile similar to the intensity distribution of the filament core which is independent of the initial NIR and IR beam profiles.

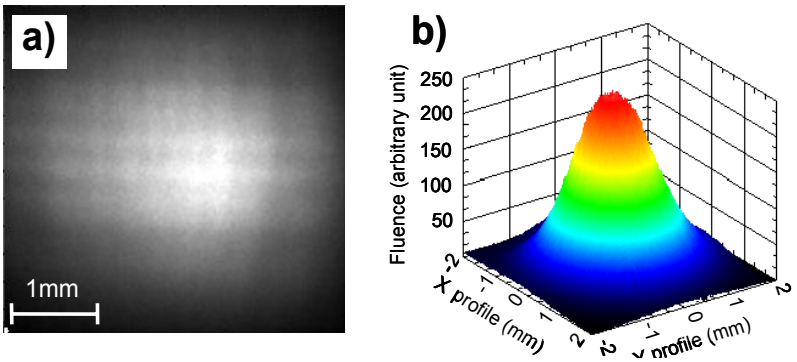

Fig. 3. Examples of (a) distorted NIR fluence distribution used to generate the filament in air and (b) the far-field fluence distribution of the generated 4WM pulse.

Figure 4 shows the temporal evolution of the measured laser pulse energies normalized to the mean energy for the NIR (Fig. 4a), IR (Fig. 4b) and the generated 4WM pulses using NIR pump power lower and higher than the critical power for self-focusing (Fig. 4c-d), respectively. The root-mean square (RMS) energy fluctuation of the input IR and NIR pulses was 1.6% and 1.5%, respectively. In the perturbative limit, one would expect a minimum RMS energy fluctuation for the generated 4WM pulse $RMS_{4WM} = 2 \times RMS_{NIR} + RMS_{IR} \cong 4.6\%$. This is indeed close to the measured value of $RMS_{4WM} = 5.2\%$ for a NIR pump power 10 times below the critical power for self-focusing in air (Fig. 4c). The measured value was slightly higher than the estimated limit because of beam pointing wondering of both the NIR and IR laser pulses. But, as we increased the NIR pump power above the critical power for self-focusing in air, we observed a stabilization of the 4WM energy fluctuation (Fig. 4d) and measured a RMS fluctuation of $RMS_{4WM,fil} = 1.8\%$, which is 3 times lower than the perturbative limit. The intensity/energy fluctuation of the reservoir of the NIR filament is similar to that of the input NIR beam before filamentation because there is no saturation mechanism occurring in the reservoir. The IR pulse did not undergo self-focusing and hence its fluctuation would remain the same during the whole interaction process. Thus, the stabilization of the 4WM energy is due to the clamping of the laser intensity inside the filament core

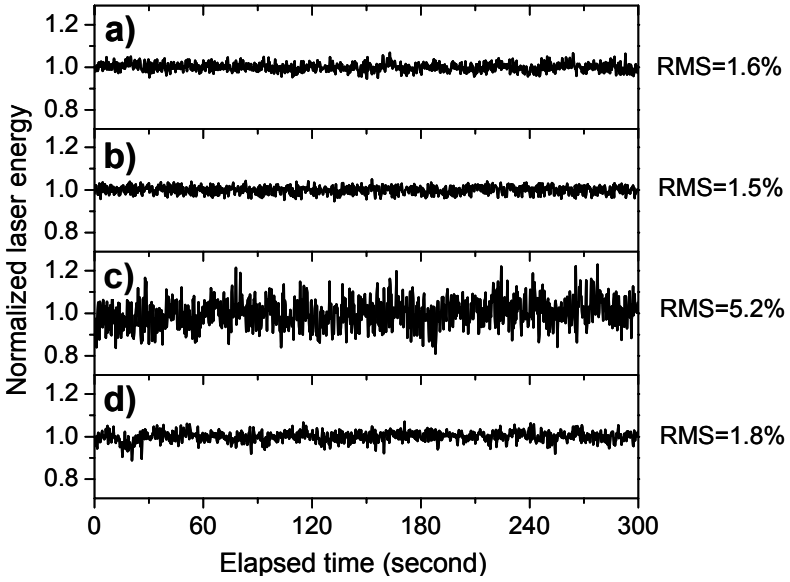

Fig. 4. Temporal evolution of energy per pulse normalized over the mean energy for (a) the IR seed, (b) the NIR pulse, (c) the generated 4WM pulse for NIR pump power (P_{NIR}) 10 times below the critical power for self-focusing (P_{cr}) in air and (d) the generated 4WM pulse for pump power above the critical power for self-focusing in air ($P_{NIR} = 2.5P_{cr}$). The root mean square (RMS) energy fluctuations are indicated on the right-hand side.

where the 4WM pulse is generated. As a consequence, even a large fluctuation of the initial NIR energy results in a constant intensity inside the filament. We estimate the maximum intensity fluctuation of the 800nm NIR pulse inside the filament from $RMS_{NIR,fil} = (RMS_{4WM,fil} - RMS_{IR})/2 = (1.8\% - 1.6\%)/2$ to be about 0.1% where the subscript 'fil' refers to filamentation. This corresponds to an indirect measurement of the stability of intensity clamping.

4.3 Condensed media

Since filamentation is a universal phenomenon in any optical medium, we should be able to sample the filament core in condensed matters, for example. In fact, this is exactly the case in glass in which waveguides have been written [24-26]. Waveguide writing in glass based upon self-focusing and filamentation is a highly nonlinear process which depends on multiphoton excitation of electrons from the valence to the conduction bands [27] following by inverse Bremsstrahlung and some collisional ionization [9], melting [28] and re-solidification/densification [29]. Thus, it is only the filament core where the intensity is high enough that has been sampled by the interaction. It is thus expected that the cross section of the waveguide would be circular similar to the cross section of the fundamental mode. Indeed, the resulting waveguide written longitudinally in fused silica using a 1 kHz repetition rate Ti-sapphire laser (45 fs, a few μJ per pulse whose power is higher than the critical power for self-focusing) is shown in Fig. 5. The cross section of the waveguide is circular in shape [26] testifying that the excellent beam quality of the filament core has been sampled.

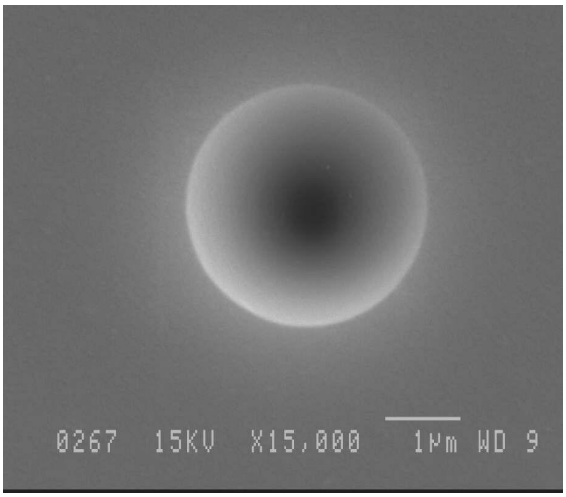

Fig. 5. Cross section of a single wave guide written in fused silica.

4.4 Third-harmonic generation: limitation due to phase mismatch

Depending on the particular nonlinear interaction inside the core, sometimes, it is not trivial to extract the nonlinear optical signal generated inside the core without destroying partially its excellent quality. Third-harmonic generation is an example. Recently, theoretical and experimental results have demonstrated that during Ti-sapphire femtosecond laser filamentation in air an ultrashort third-harmonic (TH) pulse is generated forming a two-colored filament [30]. This two-color filamentation effect is due to a nonlinear intensity-dependent phase-locking between the fundamental and the TH pulses which could extend the phase-matching over longer propagation distance inside the filament. However, it is known that the TH generated inside the filament destructively interferes with the TH generated after the filament. This is the result of the Guoy phase shift in which the TH energy generated in the filament is given back to the pump [31]. The *linear* wave-vector mismatch between the pump and the third-harmonic is much larger than that between the NIR, IR and the 4WM pulse described above. Thus the distance to decouple the fundamental and the third-harmonic laser pulses beyond the filament is critical for the measurement of the TH energy stability and TH beam profile inside the filament. Since the laser intensity inside the filament core is above the damage threshold of the decoupling mirror, the surface reflections from a pair of wedges set at large incidence angles were used to decrease the intensity of the laser pulses on the surface and thereafter a dichroic mirror was used to suppress the fundamental laser pulse and transmit the TH beam

as shown in Fig. 6a. The beam profile of the third harmonic generated in air was then measured using a CCD camera. This experimental setup was scanned along the propagation axis and could cease the filamentation process if the first wedge was positioned inside the filament zone.

The influence of the destructive interference occurring beyond the filament is clearly observed for the TH beam profile when the fundamental and the TH pulses are decoupled at the end of the filament (Fig. 6b) or 30cm beyond the filament (Fig. 6c). The beam profile shown in Fig. 6b is smooth and almost circular while the TH beam profile in Figure 6c corresponds to a central spot surrounded by a complex ring structure. The evolution of the TH beam profile clearly shows that the interaction between the fundamental and the TH pulses (energy being returned by the TH to the fundamental) beyond the filament did occur and induced severe distortions of the TH pulse's spatial quality. The distortion is small at the beginning (Fig. 6b) and becomes more severe at longer distances from the filament's end (Fig. 6c).

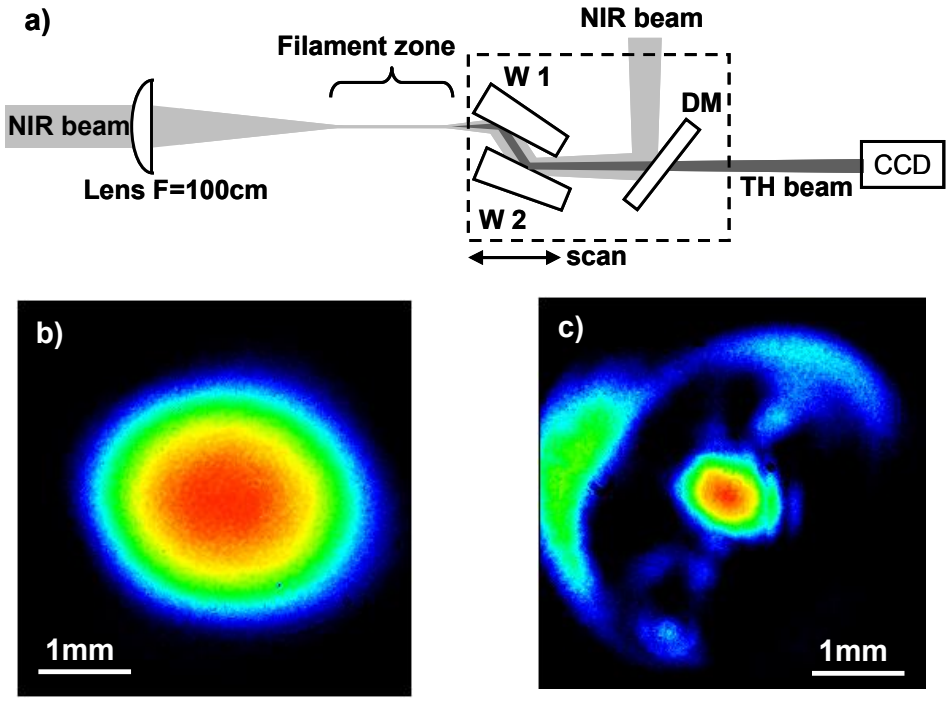

Fig. 6. (a) Experimental setup for decoupling the fundamental and TH pulses. (W) wedge, (DM) dichroic mirror. Third harmonic profiles taken by CCD camera at different positions of the dichroic mirror (b) inside the filament at z = 98cm and (c) beyond the filament at z = 128cm.

The TH energy stability was measured by replacing the CCD camera in Fig. 6a by a calibrated photomultiplier tube. Fig. 7 shows the temporal evolution of the generated third-harmonic pulse energies normalized to the mean energy for a position before the filament (Fig. 7a), inside the filament (Fig. 7b) and beyond the filament (Fig. 7c). The root-mean square (RMS) energy fluctuation of the input NIR pulses was 1.5% and in the perturbative limit, one would expect a minimum RMS energy fluctuation for the generated third-harmonic pulse to be $RMS_{TH} = 3 \times RMS_{NIR} \cong 4.5\%$. This corresponds to the measured value of $RMS_{TH} = 4.5\%$ before the filament (Fig. 7a). However, when the decoupling mirror was inside the filament zone, we observed a stabilization of the third-harmonic energy fluctuation (Fig. 7b) and measured a value of $RMS_{TH,fil} = 1.8\%$, which is 2.5 times lower than the perturbative limit. Beyond the filament, the TH energy fluctuation increased to a value of $RMS_{TH} = 3.7\%$ due to the destructive interference with some TH generated after the filament. The stabilization of the third-harmonic pulse energy inside the filament is again due to intensity

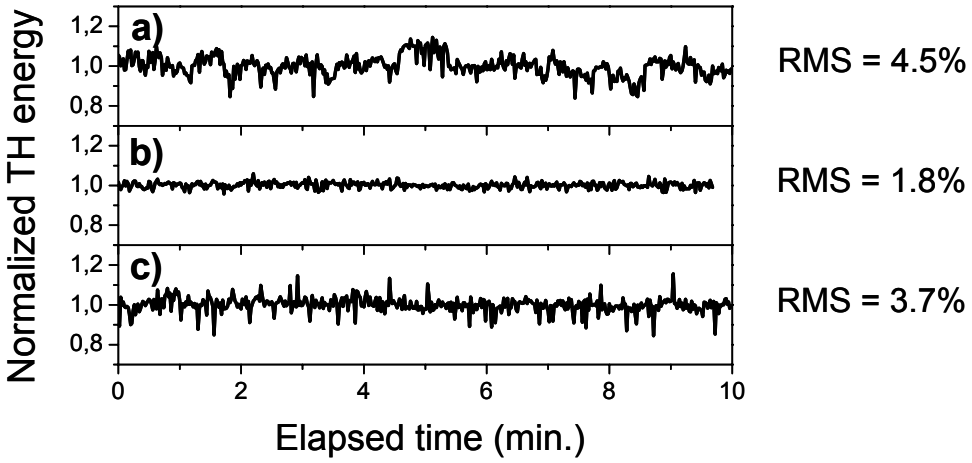

Fig. 7. Temporal evolution of third harmonic energy per pulse normalized over the mean energy (a) before the filament at z = 80cm, (b) inside the filament at z = 95cm and (c) beyond the filament at z = 110cm. The root mean square (RMS) energy fluctuations are indicated on the right-hand side.

clamping. Considering the non-negligible interaction of the fundamental and TH pulses between the first wedge and the decoupling mirror, we estimated that the maximum intensity fluctuation of the NIR pulse inside the filament $RMS_{NIR,fil} = (RMS_{TH,fil})/3 = 1.8\%/3$ was lower than 0.6%, which corroborates the measurement done for the 4MW generation.

4.5 Intrinsic limitations of self-stabilization

The above shows examples show examples of self-stabilization of the laser pulse energy inside the filament. However, it is important to note that there are intrinsic limitations about the self-stabilization of the laser pulse parameters during the filamentation. Recently, it has been observed that the filament diameter is not constant when the initial peak power changes: the filament diameter increases as a function of the initial pump power because of the counterbalance between the laser energy confined by the external focusing and the defocusing effect of the plasma [32, 33]. On the other hand, as the pump power increases, the filament length increases: thus the spectral broadening is more pronounced [34] and the pulse duration decreases [35]. In the previous sections we demonstrated that the filamentation can stabilize the energy of the generated third-harmonic pulse, but if the filament diameter and the pulse duration are not stable when the initial pump power changes, there is one question which needs to be answered: how can the filamentation stabilize the energy of the laser pulse? The physical reason for the self-stabilization of the energy inside the filament core can be explained by the theoretical model for the two-color filamentation in air described by the coupled equations given in equations (1-3) of Ref. [30]. The propagation equations include geometrical focusing, diffraction, group-velocity dispersion, self-focusing, plasma generation via multiphoton ionization and third-harmonic generation. For the numerical simulations we have considered the propagation of a linearly polarized, collimated Gaussian input laser pulse with a central wavelength at λ_0 = 807nm which is focused with a 100cm focal length lens in air at atmospheric pressure. We have used laser input powers, P_0, above the effective critical power, $P_{cr} = \lambda_0^2 / 2\pi\, n_\omega n_2$ = 8GW needed for self-focusing in air [36] and an initial beam radius of w_0 = 2mm (at $1/e^2$ of intensity). In order to verify the stability of the laser pulses in the numerical simulations, we have performed a series of calculations, in which the initial pump parameters are varied. The initial pump pulse duration, energy and peak power of 40fs, 680μJ and 16GW, were used respectively, with a root-mean-square fluctuation of 1.5%.

For an initially fixed pulse duration, the results of simulations in Fig. 8 show that the pulse durations of both the NIR and TH pulses decrease as a function of the initial peak power while their beam diameters increase inside the filament. Thus,

both the cross-section of the filament and the laser pulse duration are not stabilized during the filamentation as observed previously. However, as shown in Fig. 8, these parameters are anticorrelated and their product $\phi_{eff}^2 \times \tau_{eff}$, which corresponds in fact to the effective 'volume' of the laser pulse, is stable in Fig. 8c (for the pump pulse) and Fig. 8d (for the TH pulse) for small variations of the initial NIR peak power. It is important to note that the effective diameter and pulse duration of the fundamental pulse shown in Fig. 8a are affected by the noisy energy reservoir surrounding the filament core. On the order hand, the third-harmonic pulse is generated inside the constant (clamped) high intensity zone of the filament core. Thus, the effective diameter and pulse duration of the third-harmonic pulse, shown in Fig. 8b, are not affected by this noisy energy reservoir. The RMS fluctuation of the product $\phi_{3\omega}^2 \times \tau_{3\omega}$ is 0.2% and, hence, lower than the corresponding value of 0.9% in case of the pump pulse. Thus, the stabilization of the laser pulses energy inside the filament core are the results of intensity clamping of the pump pulse and a constant 'volume' of the laser pulses due to the dynamic equilibrium between the nonlinear intensity dependent Kerr effect and the defocusing effect of the low density plasma. Nevertheless, from the statistical analysis of numerical simulations we observe that the pulse duration fluctuation is not improved during the filamentation and becomes slightly higher than its initial value.

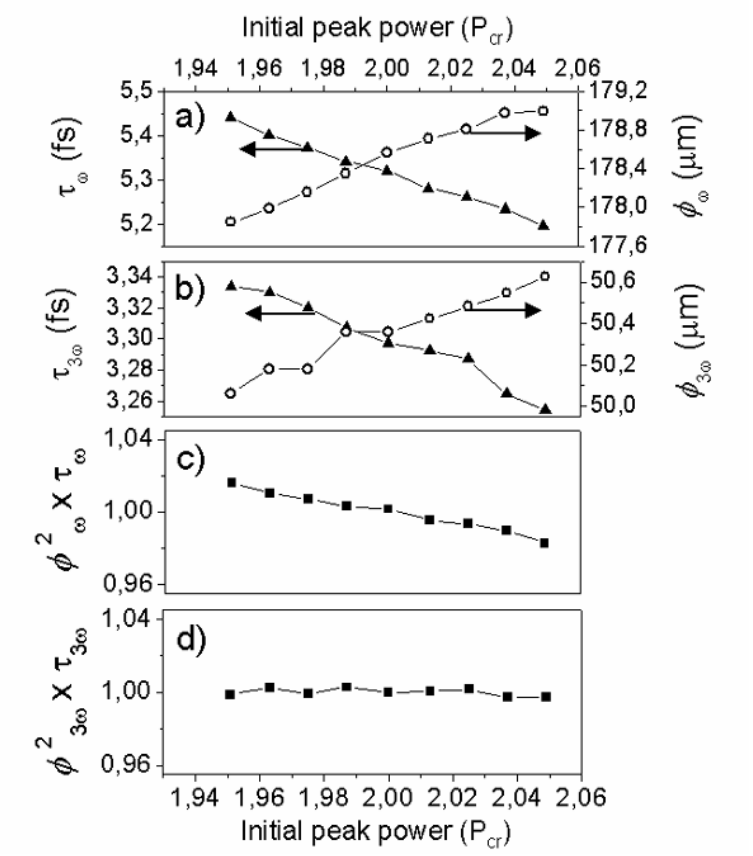

Fig. 8. Numerical results of the FWHM pulse duration (τ) and the FWHM diameter (ϕ) inside the filament at z=96cm for (a) the pump pulse and (b) the third-harmonic pulse as a function of the initial pump peak power. The product $\phi_{\omega}^2 \times \tau_{\omega}$ (arb. units) for the fundamental pulse and the product $\phi_{3\omega}^2 \times \tau_{3\omega}$ (arb. units) for the third-harmonic pulse are shown in (c) and (d), respectively, as a function of the initial pump peak power.

5. REMOTE CONTROL OF FILAMENTATION

When a powerful femtosecond laser pulse propagates in air, the peak intensity inside the filament is limited to ~5×10^{13} W/cm^2 due to the phenomenon of intensity clamping. The latter arises because of the dynamic balance between Kerr

self-focusing and defocusing of plasma produced by multiphoton/tunnel ionization of the air molecules. Such filamentation can also be generated as far as a few kilometers in the atmosphere [17]. The method we propose below is to utilize the high intensity inside the filaments to dissociate/ionize gas molecules, to explode dust particles and aerosols or to induce partial breakdown on solid targets. However, the fluorescence radiation induced by the filamentation from a collimated femtosecond laser beam fluctuates significantly on a shot-to-shot basis despite the rather stable laser pulse energy. By fluctuation, we mean that the signal intensity distribution along the propagation path as well as the starting point of the filamentation varied randomly [38]. The physical origin of these fluctuations in the fluorescence signal can be attributed to a competition among multiple filaments, which can originate from inhomogeneous intensity distribution in the transverse cross section of the pulse, due to either initial laser imperfection or previous propagation through any non-homogeneous optical medium, ultimately leading to the formation of multiple filaments co-propagating in air. Therefore, it is of particular importance to develop technology for stabilization and enhancement of the signals induced by multiple filamentation and to understand the physics of filamentation for the formation and control of filamentation to a designated distance.

We invented an effective and reliable method to merge the multi-filaments into its geometrical focus for signal enhancement and also to master the filament location in air to a remote distance [39]. We found that in a practical terawatt level laser pulse the unavoidable hot spots in the beam profile will self-focus in air at a short distance [38]. The short distance cannot be changed significantly by only controlling the chirp or divergence. We overcome such early self-focusing by using a telescope, which enlarges the diameter of the beam, thus that of the hot spots. The telescope's effective focal length is much shorter than the self-focusing distance of both the enlarged beam and the hot spots. Under this condition, the resulting multi-filaments merge into the geometrical focus, which is adjustable by varying the relative distance between the divergent and convergent optical components, as shown in Fig. 9. Since in our experimental scheme filamentation starts near the geometrical focus and the beam size is small at this position, the more effective usage of the background energy in the small beam results in consistent and strong fluorescence signals.

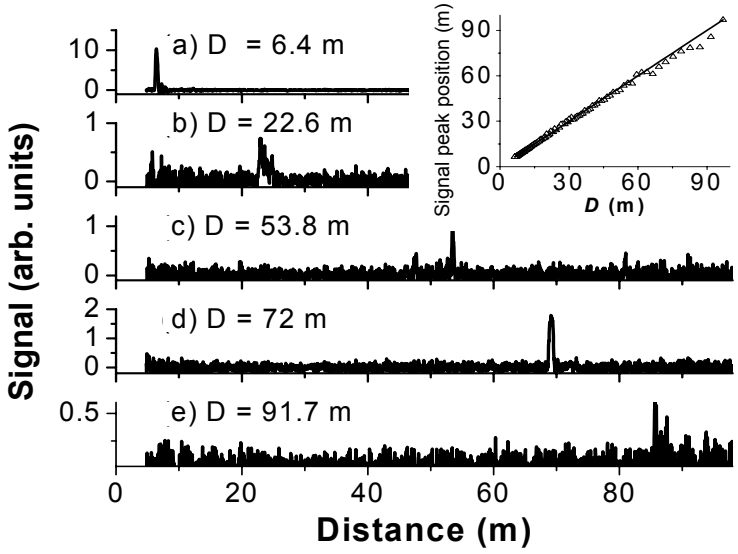

Fig. 9. Lidar collected 337 nm signals as function of the distance for different sending telescope configurations. *D* indicates the distance between the sending telescope and the calculated geometrical focus position. Inset: comparison between the measured fluorescence peak position (open triangles) and the calculated geometrical focus (solid line: slope = 1).

6. DETECTION OF CHEMICAL AND BIOLOGICAL AGENTS IN AIR

Based on the technology developed and the understanding of the filamentation physics [1, 23, 40, 41], we performed the spectroscopic study of the interaction of the filaments with different targets including gases, vapors, solids and aerosols,

in order to show the feasibility that intense femtosecond laser pulses could be applied to remote sensing of chem-bio agents.

6.1. Molecules in the gas/vapor phase

In ref. [42], the fluorescence spectrum of ethanol vapor induced by the filamentation in air has been recorded as the fingerprint of the molecules. Ethanol was selected because it is not harmful for human health when compared with most of the hydrocarbon molecules which are toxic and unsuitable for open-air experiments in the laboratory. This is the first observation of back-scattered fluorescence from the hydrocarbon pollutants from a significant laboratory scale distance (30 m), but with a constant concentration of 6.8%. Therefore, in Ref. [43], we design a long vacuum tube (4.5 m) for sensing greenhouse hydrocarbon gas methane. The reason for designing this long vacuum tube is to be able to electronically gate out the scattered white light induced by the last window of the tube and to allow spectral measurement over a reasonable period of time after the passage of the laser pulse. Backward fluorescence form dissociated CH radicals is used to quantitatively analyze the concentration of CH_4 and its remote detection limit (Fig. 10). The estimation based on the experimental results shows that the concentration sensitivity could be down to the ppm range, and the detection range limit could extend up to kilometer range. The dissociation mechanism of CH_4 has been discussed in Ref. [44]. Briefly, the intense laser field, at an intensity around or above 10^{14} W/cm^2, weakens the molecular chemical bonds and causes polyatomic molecules to dissociate into small neutral fragments through the excitation of super-excited states of the molecule. The tetrahedral methane molecule thus undergoes a stepwise disintegration. The hydrogen atoms are individually cleaved from the CH_4 molecule resulting in the production of excited CH radicals, which fluoresce.

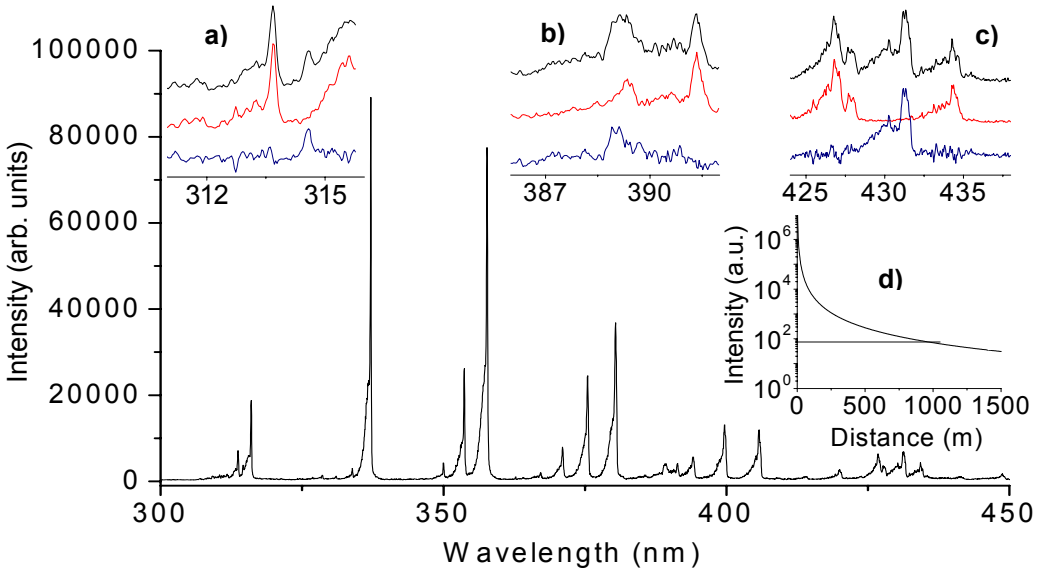

Fig.10. Filament-induced fluorescence spectrum of mixture of CH_4 and air with a CH_4 concentration of 2.6% (volume/volume). The insets (a, b and c) show the spectra in a higher resolution (top), the spectra of pure air in atmospheric pressure (middle), and the subtraction of the mixture and pure air spectra (bottom). The bands are (a) CH: C $^2\Sigma^+$ - X $^2\Pi$, (b) CH: B $^2\Sigma^-$ - X $^2\Pi$, and (c) CH: A $^2\Delta$ - X $^2\Pi$. The inset (d) shows the extrapolation of the detection limit according to the LIDAR equation ($I=L/R^2$, where I is the signal intensity, L the effective filament length and R the distance between the end of the filament and the detector). The detection limit is about 0.9 km for the CH_4 concentration of 5% and the filament length of 20 m.

6.2. Biological targets

For the detection of solid biological samples, we have experimentally shown the remarkably distinct spectra of egg white and yeast powders using time-resolved filament-induced breakdown spectroscopy (FIBS) [45]. In particular, we

demonstrated the feasibility of remote detection and differentiation of some very similar agriculture related bioaerosols, namely barley, corn, and wheat grain dusts using this technique [46]. The signals were detected in LIDAR configuration. All the species showed identical spectra, namely those from molecular C_2 and CN bands, as well as atomic Si, C, Mg, Al, Na, Ca, Mn, Fe, Sr and K lines. These identical spectral bands and lines reveal similar chemical compositions; however, the relative intensities of the spectra are different showing different element abundances from these three bio-targets. The intensity ratios of different elemental lines were used to distinguish these three samples.

6.3. Water aerosols containing metallic salts

We have also demonstrated that the usage of a simple telescope as sending optics (see Ref. 39) could greatly improve the performance of remote FIBS (R-FIBS) for probing a cloud of microdroplets where table salt has been dissolved [48]. These microdroplets are a good simulant for aerosols. We demonstrated experimentally in Figure 11 that R-FIBS can efficiently be used as a ppm level sensing technique to remotely retrieve composition of microdroplets in clouds located at a distance. The technique has been successfully tested up to 70 m and, as revealed by extrapolation, showed great potential for kilometer range application. This technique is sensitive to the solvent as well. Four hydrogen bands from the Balmer series were observed in aqueous microdroplet cloud after H_2O molecules were broken by the light filaments. Additionally, a cloud of aqueous aerosols containing a mixture of $PbCl_2$, $CuCl_2$, $FeCl_2$ and NaCl has also been detected using R-FIBS [49]. It was found that fluorescence from all the metallic ions dissolved can be observed (Fig. 11). Moreover, these spectrally narrow atomic transitions excited by the low density plasma did not show any signal overlap.

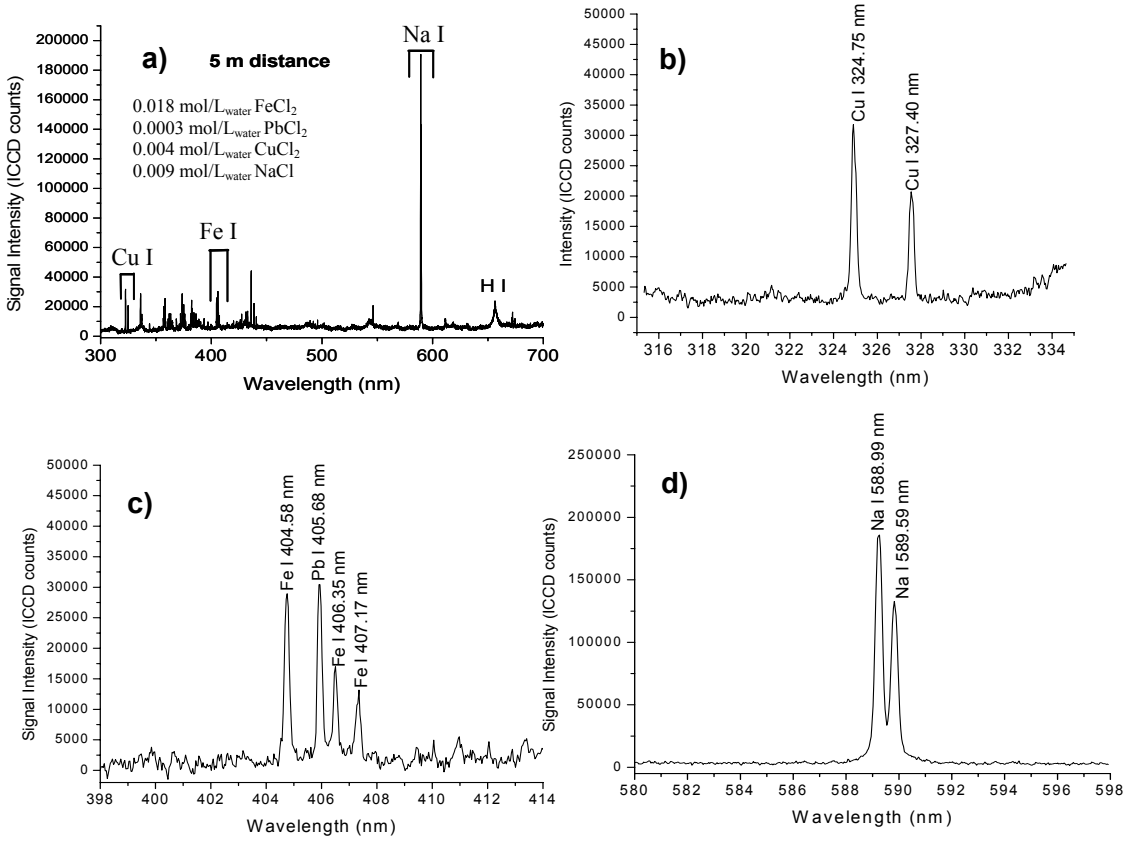

Fig. 11. Typical R-FIBS spectrum a) of a thin aerosol cloud with a 95 % transmission of the 632 nm wavelength containing the listed quantities of iron dichloride, lead dichloride, copper dichloride and sodium chloride. The regions referred to as Cu I, Fe I and Na I in a) are enlarged for clarity in b), c) and d), respectively.

6.4. Metallic targets

Finally, R-FIBS was also used for metallic targets (lead, aluminum and copper) [47]. In this case, because the filaments are short, white light continuum inside R-FIBS spectrum is negligible, realizing non-gated R-FIBS. And because the filaments are strong, the resulting line emission is impressively intense. The extrapolated detection limit of the aluminum sample reaches a few kilometers in distance and a few ppm in terms of minor element concentration when the sample is located 50 m away from the detection system.

7. CONCLUSION

In the first part of this manuscript we have demonstrated that a filamenting femtosecond laser pulse self-stabilizes the energy inside the filament core due to intensity clamping and generates an excellent spatial beam quality inside the core due to self-spatial-filtering. The high quality of these natural self-improvement processes (self-stabilization and self-spatial-filtering) can be transferred to the outcome of numerous nonlinear optical interaction that can be induced efficiently (because of the high clamped intensity) inside the filament in transparent media. Furthermore, the nonlinear optical processes induced inside a filament (four-wave mixing, third-harmonic generation and other parametric processes [1]) would generate a high intensity signal that is phase locked to the filament core [30]. Since the filament core self-compresses into a few-cycle pulse, sampling this core by a nonlinear optical process would also generate few-cycle signal pulses. It is thus feasible to generate inside the filament two or more co-propagating, overlapping (phase-locked) few-cycle stable, high quality and high intensity pulses of different wavelengths.

In the case of remote filamentation of 800nm laser pulse and based on the experimental evidences, we observed “clean” fluorescence emission of chem-bio agents induced by the filaments of powerful femtosecond laser pulses in air and can indeed be used as the fingerprint to distinguish different chemical and biological agents. A single filamenting laser pulse is sufficient to induce characteristic fluorescence from a large number of molecular species. The possibility of observing many atmospheric constituents of interest is not to be questioned anymore. This allows us to extrapolate our claim that femtosecond laser filamentation would be an ‘ideal tool’ for the detection and identification of almost all if not all atmospheric chemical and biological agents/pollutants; i.e. one laser does all or almost.

8. ACKNOWLEDGEMENT

This work was partially supported by the Natural Sciences and Engineering Research Council of Canada (NSERC), Defence Research and Development Canada in Valcartier (DRDC-Valcartier), Canada Research Chair, Canada Foundation for Innovation (CFI), Canadian Institute for Photonics Innovation (CIPI), le Fonds Québécois pour la Recherche sur la Nature et la Technologie (FQRNT).

REFERENCES

[1] S. L. Chin, S. A. Hosseini, W. Liu, Q. Luo, F. Théberge, N. Aközbek, A. Becker, V. P. Kandidov, O. G. Kosareva and H. Schroeder, "The propagation of powerful femtosecond laser pulses in optical media: physics, applications, and new challenges," *Can. J. Physics* **83**, 863-905 (2005).

[2] C. P. Hauri, W. Kornelis, F. W. Helbing, A. Heinrich, A. Couairon, A. Mysyrowicz, J. Biegert and U. Keller, "Generation of intense, carrier-envelope phase-locked few-cycle laser pulses through filamentation," *Appl. Phys. B* **79**, 673-677 (2004).

[3] C. P. Hauri, A. Guandalini, P. Eckle, W. Kornelis, J. Biegert and U. Keller**,** "Generation of intense few-cycle laser pulses through filamentation – parameter dependence," *Opt. Express* **13**, 7541-7547 (2005).

[4] X. Chen, Y. Leng, J. Liu, Y. Zhu, R. Li and Z. Xu, "Pulse self-compression in normally dispersive bulk media," *Opt. Commun.* **259**, 331-335 (2006).

[5] A. Couairon, M. Franco, A. Mysyrowicz, J. Biegert and U. Keller**,** "Pulse self-compression to the single-cycle limit by filamentation in a gas with a pressure gradient," *Opt. Lett.* **30**, 2657-2659 (2005).

[6] A. Couairon, J. Biegert, C. P. Hauri, W. Kornelis, F. W. Helbing, U. Keller and A. Mysyrowicz, "Self-compression of ultra-short laser pulses down to one optical cycle by filamentation, "*Journal of Modern Optics,* **53**, 75-85 (2006).

[7] S. L. Chin, S. Petit, F. Borne and K. Miyazaki, "The white light supercontinuum is indeed an ultrafast white light laser," *Jpn. J. Appl. Phys.* **38**, L126-128 (1999).
[8] S. L. Chin, A. Brodeur, S. Petit, O. G. Kosareva and V. P. Kandidov, "Filamentation and supercontinuum generation during the propagation of powerful ultrashort laser pulses in optical media (white light laser)," *Journal of Nonlinear Optical Physics and Materials* **8**, 121-146 (1999).
[9] V. P. Kandidov, O. G. Kosareva, I. S. Golubtsov, W. Liu, A. Becker, N. Akozbek, C. M. Bowden and S. L. Chin, "Self-transformation of a powerful femtosecond laser pulse into a white-light laser pulse in bulk optical media (or supercontinuum generation)," *Appl. Phys. B* **77**, 149-165 (2003).
[10] F. Théberge, W. Liu, Q. Luo and S. L. Chin, "Ultrabroadband continuum generated in air (down to 230 nm) using ultrashort and intense laser pulses," *Appl. Phys. B* **80**, 221-225 (2005).
[11] J. Kasparian, R. Sauerbrey, D. Mondelain, S. Niedermeier, J. Yu, J.-P. Wolf, Y.-B. André, M. Franco, B. Prade, S. Tzortzakis, A. Mysyrowicz, M. Rodriguez, H. Wille and L. Wöste, "Infrared extension of the super continuum generated by femtosecond terawatt laser pulses propagating in the atmosphere," *Opt. Lett.* **25**, 1397-1399 (2000).
[12] M. Mlejnek, E. M. Wright and J. V. Moloney, "Dynamic spatial replenishment of femtosecond pulses propagating in air," *Opt. Lett.* **23**, 382-384 (1998).
[13] W. Liu, F. Théberge, E. Arévalo, J.-F. Gravel, A. Becker and S. L. Chin, "Experiment and simulations on the energy reservoir effect in femtosecond light filaments," *Opt. Lett.* **30**, 2602-2604 (2005).
[14] J. Kasparian, R. Sauerbrey and S. L. Chin, "The critical laser intensity of self-guided light filaments in air," *Appl. Phys. B* **71**, 877-879 (2000).
[15] A Becker, N. Akozbek, K. Vijayalakshmi, E. Oral, C. M. Bowden and S. L. Chin, "Intensity clamping and re-focusing of intense femtosecond laser pulses in nitrogen molecular gas," *Appl. Phys. B* **73**, 287-290 (2001).
[16] W. Liu, S. Petit, A. Becker, N. Aközbek, C. M. Bowden and S. L. Chin, "Intensity clamping of a femtosecond laser pulse in condensed matter," *Opt. Commun.* **202**, 189-197 (2002).
[17] M. Rodriguez, R. Bourayou, G. Méjean, J. Kasparian, J. Yu, E. Salmon, A. Scholz, B. Stecklum, J. Eislöffel, U. Laux, P. Hatzes, R. Sauerbrey, L. Wöste and J.-P. Wolf, "Kilometer-range nonlinear propagation of femtosecond laser pulses," *Phys. Rev. E* **69**, 036607 (2004).
[18] A. Brodeur, C. Y. Chien, F. A. Ilkov, S. L. Chin, O. G. Kosareva and V. P. Kandidov, "Moving focus in the propagation of powerful ultrashort laser pulses in air," *Opt. Lett.* **22**, 304-306 (1997).
[19] S. L. Chin, *From Multiphoton to Tunnel Ionization*, in *Advances in Multiphoton Processes and Spectroscopy*, S. H. Lin, A. A. Villaeys and Y. Fujimura, eds., Singapore, pp. 249, 2004.
[20] N. Aközbek, M. Scalora, C. M. Bowden and S. L. Chin, "White light continuum generation and filamentation during the propagation of ultra-short laser pulses in air," *Opt. Commun.* **191**, 353-362 (2001).
[21] S. Tzortzakis, B. Prade, M. Franco and A. Mysyrowicz, "Time-evolution of the plasma channel at the trail of a self-guided IR femtosecond laser pulse in air," *Opt. Commun.* **181**, 123-127 (2000).
[22] B. La Fontaine, F. Vidal, Z. Jiang, C. Y. Chien, D. Comtois, A. Desparois, T. W. Johnston, J.-C. Kieffer, H. Pépin and H. P. Mercure, "Filamentation of ultrashort pulse laser beams resulting from their propagation over long distances in air," *Phys. Plasmas* **6**, 1615-1621 (1999).
[23] F. Théberge, N. Aközbek, W. Liu, A. Becker and S. L. Chin, "Tunable Ultrashort Laser Pulses Generated through Filamentation in Gases," *Phys. Rev. Lett.* **97**, 023904 (2006).
[24] K. Hirao and K. Miura, "Writing waveguides and gratings in silica and related materials by a femtosecond laser," *J. Non-Cryst. Solids* **239**, 91-95 (1998).
[25] K. Miura, J. Qiu, T. Mitsuyu, and K. Hirao, "Preparation and optical properties of fluoride glass waveguides induced by laser pulses," *J. Non-Cryst. Solids* **256**, 212-219 (1999).
[26] A. Saliminia, N.T. Nguyen, M.-C. Nadeau, S. Petit, S.L. Chin and R. Vallée, "Writing optical waveguides in fused silica using 1 kHz femtosecond IR pulses," *J. Appl. Phys.* **93**, 3724-3728 (2003).
[27] A. Brodeur and S. L. Chin, "Band-gap dependence of the ultrasfast white-light continuum," *Phys. Rev. Lett.* **80**, 4406-4409 (1998).
[28] V. Koubassov , J. F. Laprise, F. Théberge, E. Förster, R. Sauerbrey, B. Müller, U. Glatzel and S. L. Chin, "Ultrafast laser-induced melting of glass," *Appl. Phys. A* **79**, 499-505 (2004).
[29] A. Saliminia, N. T. Nguyen, S. L. Chin and R. Vallée, "Densification of silica glass induced by 0.8 and 1.5 μm intense femtosecond laser pulses," *J. Appl. Phys.* **99**, 093104 (2006).

[30] N. Aközbek, A. Iwasaki, A. Becker, M. Scalora, S. L. Chin and C. M. Bowden, "Third-Harmonic Generation and Self-Channeling in Air Using High-Power Femtosecond Laser Pulses," *Phys. Rev. Lett.* **89**, 143901 (2002).
[31] R. W. Boyd, "Intuitive explanation of the phase anomaly of focused light beams," *J. Opt. Soc. Am.* **70,** 877-880 (1980).
[32] Y. P. Deng, J. B. Zhu, Z. G. Ji, J. S. Liu, B. Shuai, R. X. Li, Z. Z. Xu, F. Théberge and S. L. Chin, "Transverse evolution of a plasma channel in air induced by femtosecond laser," *Opt. Lett.* **31**, 546-548 (2006).
[33] F. Théberge,W. Liu, P. Tr. Simard, A. Becker and S.L. Chin, "Plasma density inside a femtosecond laser filament in air: Strong dependence on external focusing," *Phys. Rev. E* **74**, 036406 (2006).
[34] F. Théberge, W. Liu, S. A. Hosseini, Q. Luo, S. M. Sharifi and S. L. Chin, "Long-range spectrally and spatially resolved radiation from filaments in air," *Appl. Phys. B* **81**, 131-134 (2005).
[35] J. Liu, X. W. Chen, J. S. Liu, Y. Zhu, Y. X. Leng, J. Dai, R. X. Li and Z. Z. Xu, "Spectrum reshaping and pulse self-compression in normally dispersive media with negatively chirped femtosecond pulses," *Opt. Expr.* **14**, 979-987 (2006).
[36] W. Liu and S. L. Chin, "Direct measurement of the critical power of femtosecond Ti:sapphire laser pulse in air," *Opt. Expr.* **13**, 5750-5755 (2005).
[37] F. Théberge, Q. Luo, W. Liu, S. A. Hosseini, M. Sharifi and S. L. Chin, "Long-rang third-harmonic generation in air using ultrashort intense laser pulses," *Appl. Phys. Lett.* **87**, 081108 (2005).
[38] Q. Luo, S.A. Hosseini, W. Liu, J.-F. Gravel, O.G. Kosareva, N.A. Panov, N. Aközbek, V.P. Kandidov, G. Roy and S.L. Chin , "Effect of beam diameter on the propagation of intense femtosecond laser pulses," *Appl. Phys. B* **80**, 35-38 (2005).
[39] W. Liu, F. Théberge, J.-F. Daigle, P.T. Simard, S.M. Sarifi, Y. Kamali, H.L. Xu and S.L. Chin, "An efficient control of ultrashort laser filament location in air for the purpose of remote sensing," *Appl. Phys. B* **85**, 55-58 (2006).
[40] S.L. Chin, F. Théberge and W. Liu, "Filamentation nonlinear optics," *Appl. Phys. B* **86**, 477-483 (2007).
[41] S.L. Chin, "Some Fundamental Concepts of Femtosecond Laser Filamentation," *J. Korean Phys. Soc.* **49**, 281 (2006).
[42] Q. Luo, H.L. Xu, S.A. Hosseini, J.-F. Daigle, F. Théberge, S.M. Sharifi and S.L. Chin, "Remote sensing of pollutants using femtosecond laser pulse fluorescence spectroscopy," *Appl. Phys. B* **82**, 105-109 (2006).
[43] H.L. Xu, J.-F. Daigle, Q. Luo and S.L. Chin, "Femtosecond laser-induced nonlinear spectroscopy for remote sensing of methane," *Appl. Phys. B* **82**, 655-658 (2006).
[44] F. Kong, Q. Luo, H.L. Xu, M. Sharifi, D. Song and S.L. Chin, "Explosive photodissociation of methane induced by ultrafast intense laser," *J. Chem. Phys.* **125**, 133320 (2006).
[45] H.L. Xu, W. Liu and S.L. Chin, "Remote time-resolved filament-induced breakdown spectroscopy of biological materials," *Opt. Lett.* **31**, 1540-1542 (2006).
[46] H.L. Xu, G. Méjean, W. Liu, Y. Kamali, J.-F. Daigle, A. Azarm, P.T. Simard, P. Mathieu, G. Roy, J.-R. Simard and S.L. Chin, "Remote sensing of similar biological materials using femtosecond filament-induced breakdown spectrocospy," *Appl. Phys. B* **87**, 151-156 (2007).
[47] W. Liu, H.L. Xu, G. Méjean, Y. Kamali, J.-F. Daigle, A. Azarm, P.T. Simard, P. Mathieu, G. Roy and S.L. Chin, "Efficient non-gated remote filament-induced breakdown spectroscopy of metallic sample," *Spectrochimica Acta Part B* **62**, 76 (2007).
[48] J.-F. Daigle, G. Méjean, W. Liu, F. Théberge, H.L. Xu, Y. Kamali, J. Bernhardt, A. Azarm, Q. Sun, P. Mathieu, G. Roy, J.-R. Simard and S.L. Chin, "Long Range Trace Detection in Aqueous Aerosol using Remote Filament-Induced Breakdown Spectroscopy," *Appl. Phys. B* (accepted, 2007).
[49] J.-F. Daigle, P. Mathieu, G. Roy, J.-R. Simard and S.L. Chin, "Multi-Constituents Detection in Contaminated Aerosol Clouds using Remote Filament-Induced Breakdown Spectroscopy," *Opt. Commun.* (accepted, 2007).